Soldagem & Inspeção

ISSN 1980-6973 (Online) | ISSN 0104-9224 (Print)

TECHNICAL PAPERS

Influence of Nb Content on Sensitization and Pitting Corrosion of Welded AISI 430 Ferritic Stainless Steel

Caroline Nazaré Gonçalves[1], Gabriel Mendes de Almeida Carvalho[1,2], Jordânio Samuel Siqueira[3], Reny Ângela Renzetti[3]

[1] Universidade Federal de Minas Gerais – UFMG, Belo Horizonte, MG, Brasil.
[2] Instituto Federal de Minas Gerais – IFMG, Ibirité, MG, Brasil.
[3] Universidade Federal de Itajubá – UNIFEI, Itabira, MG, Brasil.

Como citar: Gonçalves CN, Carvalho GMA, Siqueira JS, Renzetti RA. Influence of Nb content on sensitization and pitting corrosion of welded AISI 430 ferritic stainless steel. Soldagem & Inspeção. 2019;24:e2421. https://doi.org/10.1590/0104-9224/SI24.21

Abstract: In this work, the effect of Nb addition on sensitization and pitting corrosion of welded AISI 430 ferritic stainless steel subjected to autogenous GTAW was investigated by microstructural characterization and electrochemical techniques. The three distinct regions of welding process, weld metal, heat affected zone and base metal of AISI 430 steel with and without Nb were evaluated. The degree of sensitization was measured by double loop electrochemical potentiodynamic reactivation and pitting corrosion was studied by potentiostatic polarization test. The microstructural analyses reported martensite network in the weld metal and heat affected zone of AISI 430 non stabilized. The electrochemical studies revealed that the highest degree of sensitization and the lowest pitting potential are in the weld metal of AISI 430 without Nb.

Key-words: Degree of sensitization; Pitting corrosion; Ferritic stainless steel; Nb; GTAW.

Influência da Adição de Nb na Sensitização e Corrosão por Pite do Aço Inoxidável Ferrítico AISI 430 Soldado

Resumo: Neste trabalho, o efeito da adição de Nb na sensitização e corrosão por pite de aço inoxidável ferrítico AISI 430 submetido à soldagem TIG foi investigado por caracterização microestrutural e técnicas eletroquímicas. As três regiões distintas do processo de soldagem, zona fundida, zona termicamente afetada e metal de base do aço AISI 430 com e sem Nb foram avaliadas. O grau de sensitização foi medido por reativação potenciodinâmica eletroquímica de "double loop" e a corrosão por pite foi estudada por testes de polarização potenciostática. As análises microestruturais revelaram uma fase martensítica na zona fundida e zona termicamente afetada do AISI 430 não estabilizado. Os estudos eletroquímicos mostraram que o maior grau de sensitização e o menor potencial de pite estão na zona fundida do aço sem adição de Nb.

Palavras-chave: Grau de sensitização; Corrosão por pite; Aço inoxidável ferrítico; Nb; TIG.

1. Introduction

The commercial AISI 430 ferritic stainless steels are widely used due to their good strength and ductility and good corrosion resistance in caustic and chloride environments. Since the early 80s, the applications of this steel have expanded dramatically and nowadays they have been applied in automotive exhaust systems, combustion chambers, and furnace parts. For some of these applications, welding is the major fabrication process utilized.

Gas tungsten arc welding (GTAW) also known as tungsten inert gas (TIG) is an arc welding process that produces very high quality welds in ferritic stainless steels. However, the heat applied results in microstructural changes and influences the mechanical and corrosion properties. The weld metal (WM) and heat affected zone (HAZ) obtained by the welding process exhibit undesirable grain growth and precipitation of secondary phases, including the precipitation of chromium rich constituents, which contributes to low toughness and ductility and to reduce the corrosion resistance of the steel [1-5].

The precipitation of chromium-rich carbides in the vicinity of grain boundaries is a consequence of the heat input and can be present in the WM and HAZ of welded steel. Adjacent to the carbides, chromium concentration is reduced and sensitization and possible intergranular corrosion may occur.

In order to improve its weldability, by minimizing mechanical and corrosion resistance losses, it is usual to add stabilizing elements, mainly niobium. It has been noticed that the presence of this element stabilizes C and N, i.e. to remove C and N

Received: 30 Oct., 2018. Accepted: 29 July, 2019.
E-mails: carolgoncalves92@hotmail.com (CNG), gmendescarvalho@gmail.com; gabriel.almeida@ifmg.edu.br (GMAC), jordaniosamuel@hotmail.com (JSS), renzetti.ra@gmail.com (RAR)

from the solid solution, owing to their strong tendency to form carbide and nitride precipitates, inhibiting the formation of chromium-rich carbides at the matrix and grain boundaries of the steel [6-9].

The main goal of this study was to investigate through electrochemical techniques and microstructural characterization the effect of the Nb addition in the sensitization and pitting corrosion resistance of a welded AISI 430 ferritic stainless steel.

2. Methodology

The chemical compositions of the previously annealed ferritic stainless steels, AISI 430A and AISI 430E, investigated in this study are given in Table 1. For the same steel, two cold rolled 0.6 mm thick sheets were welded by using TIG process (power source: INVERSAL 300 IMC). The weld metal was performed without metal addition (autogenous welding) and in argon shielding gas with 8 L/min gas flow.

Table 1. Chemical composition of AISI 430A and AISI 430E (in %.wt).

	C	Mn	Si	Cr	Ti	Nb	N	P	S
430 A	0.043	0.289	0.244	16.251	0.008	0.041	0.038	0.040	0.015
430 E	0.021	0.239	0.290	16.321	0.011	0.358	0.02	0.035	0.016

The test bench, shown in Figure 1, is composed of a displacement device (Tartilope V1 IMC) coupled to a copper plate where the specimens to be welded are placed. This configuration allows a precise adjustment of the welding speed with the stationary torch. In addition, a clamping device adjusts torch-to-sample positioning, keeping the distance between the electrode and sample (arc length) constant and similar for all tests.

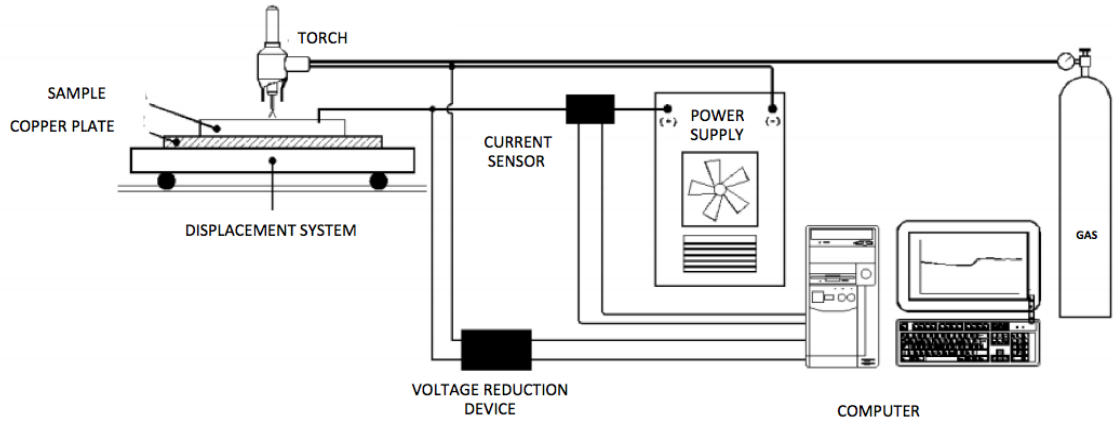

Figure 1. Scheme of the welding components and acquisition system.

The distance between the electrode and the samples for all tests was 2 mm and the value of the electric current set (*I*) at 120 A, the voltage values (*V*) acquired were between 11.0 and 13.0 V and an average of 12.0 V. In order to obtain the same welding energy, the welding speed (*v*) was set at 4.17 mm / s for all the specimens.

Thus, through Equation 1 it is possible to calculate the welding energy in this autogenous process of the TIG welding, which was 0.345 kJ / mm applied in all the samples. A scheme of the weld bead and the rejected regions (extremities of the plates) is shown in the Figure 2. The 15 mm of both extremities of the plates were eliminated in order to avoid any instability that could appear during the process.

$$H = \left(\frac{1}{vT}\right)\int_0^T VIdt \approx \frac{VI}{v} \quad (1)$$

where T = temperature; t = time.

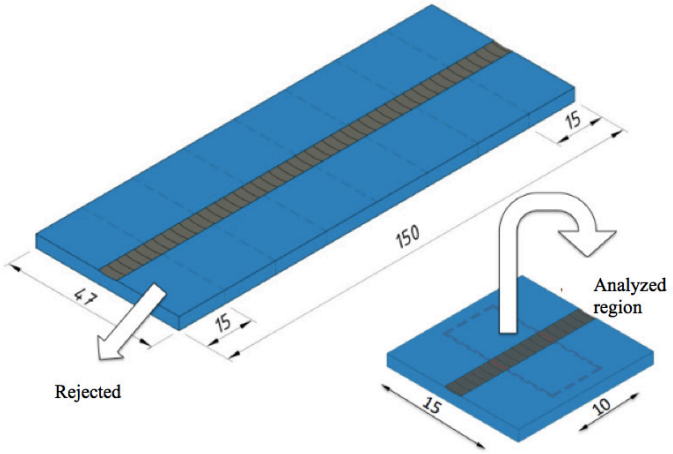

Figure 2. Scheme of the weld bead in the plate and the analyzed section.

The welding process effects on the microstructure of ferritic stainless steels were studied by optical metallography Leitz Model Metallux and the images were registered in a Digital Leica DFC camera. Specimens were cut as shown in Figure 2 and prepared using standard metallographic procedure, polished with diamond paste of 1 µm. Microstructural characterization of the weld beads and identification of the microconstituents present were performed using Vilella reagent (1 g of picric acid + 5 mL of hydrochloric acid + 100 mL of ethyl alcohol).

The electrochemical techniques were performed separately on the resulting regions from welding process base metal (BM), HAZ and WZ. For the same welded steel, three samples of each region were mounted in epoxy resin and the regions were carefully separated according to the microstructure and microhardness values. A synthetic-resin was used to separate the interface between sample and epoxy resin in order to avoid crevice corrosion and to isolate the regions. The Emstat^3+ potentiostat (Palm Sens™) was utilized. The samples were ground to 600 grit paper prior testing.

In the quantitave evaluation of susceptibility to intergranular corrosion, the Double Loop Electrochemical Potentiodynamic Reactivation (DL-EPR), was used 1M H_2SO_4 in distilled water solution. The samples were immersed during 300 s in the open circuit potential, followed by anodic polarization until 300 mV with a scanning rate of 1.67 mV/s. Upon reaching the potential in the passive state; the polarization scan was reverted back to the open circuit potential with the same scanning rate. The value of current density, Ia (anodic activation current) and Ir (anodic reactivation current) were obtained directly from the curve with the aid of Origin® software. The degree of sensitization (DOS) was calculated by the ratio (Ir/Ia). The saturated calomel electrode (SCE) was used as reference electrode. The counter electrode consisted of a platinum rod. The working electrode was the samples themselves embedded in the epoxy resin and attached to an insulated copper contact wire that was connected to the potentiostat. Measurements were made in triplicates to ensure assay reproducibility. The specimens of the DL-EPR were also examined by scanning electron microscopy (SEM).

Pitting corrosion of the regions was conducted from -150 to 100 mV at a scan rate of 0.0005 V/s in 3.5 wt.% sodium chloride in distilled water. All the electrochemical experiments were conducted at room temperature.

3. Results and Discussion

3.1. Microstructure characterization

The microstructure of welded AISI 430A is shown in Figure 3a-c and AISI 430E in Figure 3d-f, being shown Figure 3a and 3d for BM; Figure 2b and 3e for HAZ; Figure 3c and 3f for WM.

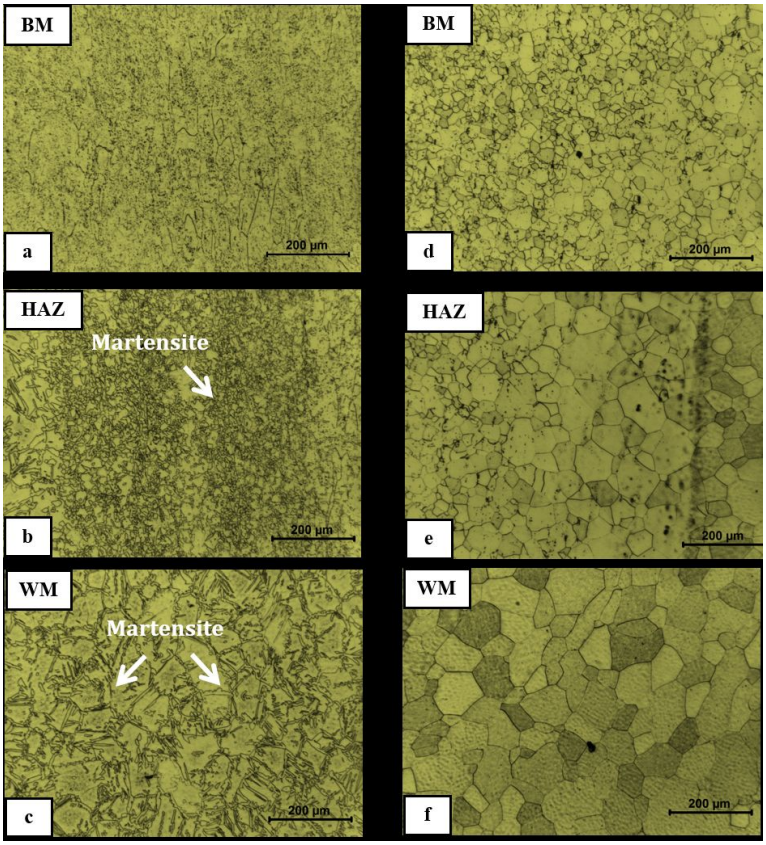

Figure 3. BM (a), HAZ (b) and WM (c) of the AISI 430A; BM (d), HAZ (e) and WM (f) of the AISI 430E.

The WM and HAZ of AISI 430A steel, Figure 3b, c showed martensite net adjacent to the grain boundaries of the ferrite matrix and possible fine precipitates of $M_{23}C_6$. Figure 4 shows a SEM of the welded metal of the AISI 430A presenting ferrite and martensite microstructure. In the HAZ the martensite net were found denser. This microstructure is justified by the high levels of (C+N) that induce the formation of austenite at high temperatures, even at high contents of chromium. Thus, during welding, the steel has undergone to partial transformation of the ferrite at high temperatures presenting a biphasic microstructure, austenite + ferrite, and after the fast cooling ferrite + martensite microstructure [5,10,11]. The resulting microstructure of AISI 430 can also be predicted by the Kaltenhauser Ferrite Factor (KFF) [12], which evaluates the tendency to form martensite in a ferritic stainless steel through the balance of alphagenic and gammagenic elements (Equation 2):

$$KFF = Cr + 6 \cdot Si + 8 \cdot Ti + 4 \cdot Mo + 2 \cdot Al - 40 \cdot (C + N) - 2 \cdot Mn - 4 \cdot Ni \quad (2)$$

The AISI 430A steel has a KFF of 14.9 lower than the minimum value of 17 where the formation of austenite at high temperature and martensite after cooling is not expected. In this way, the resulting biphasic microstructure is in agreement with the predicted by this equation.

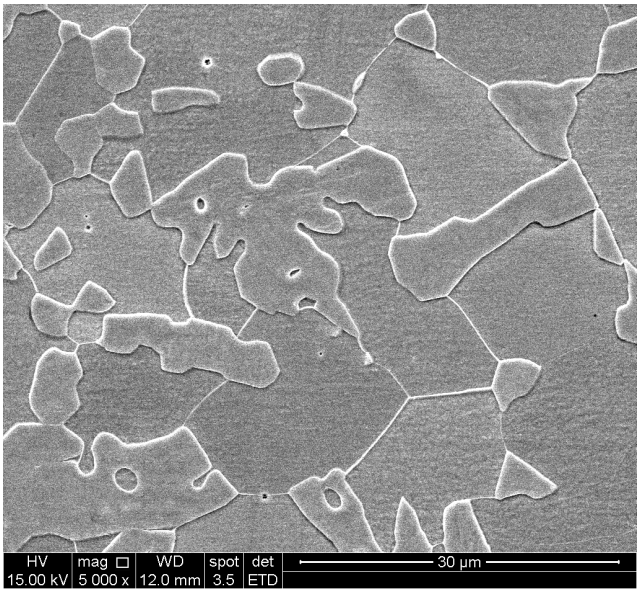

Figure 4. SEM of AISI 430A steel. F: Ferrite. M: Martensite.

The stabilized ferritic stainless steel with Nb AISI 430E showed a completely ferritic microstructure in the WM, HAZ and BM, Figure 3d-f. The addition of the ferrite stabilizing element has reduced and/or inhibited the field of austenite existence. This is justified by the fact that this element partially or completely replaces the carbides and nitrides of Cr by carbonitrides of Nb (C, N). An EDS analysis of AISI 430E has confirmed the presence of precipitates inter and intragranular with a high content of Nb, Figure 5, which based in the literature are NbC precipitates [13,14]. These precipitates are more stable than Cr and less soluble and only dissolve in the ferritic matrix at temperatures above 1200 °C. By limiting the dissolution of both C and N in the ferrite at elevated temperatures the stabilizer reduce the effect of the austenite stabilizing elements and limit and/or prevent the formation of austenite between 900 and 1200 °C [2]. Thus, the properly stabilized steel presented a completely ferritic microstructure after the welding process.

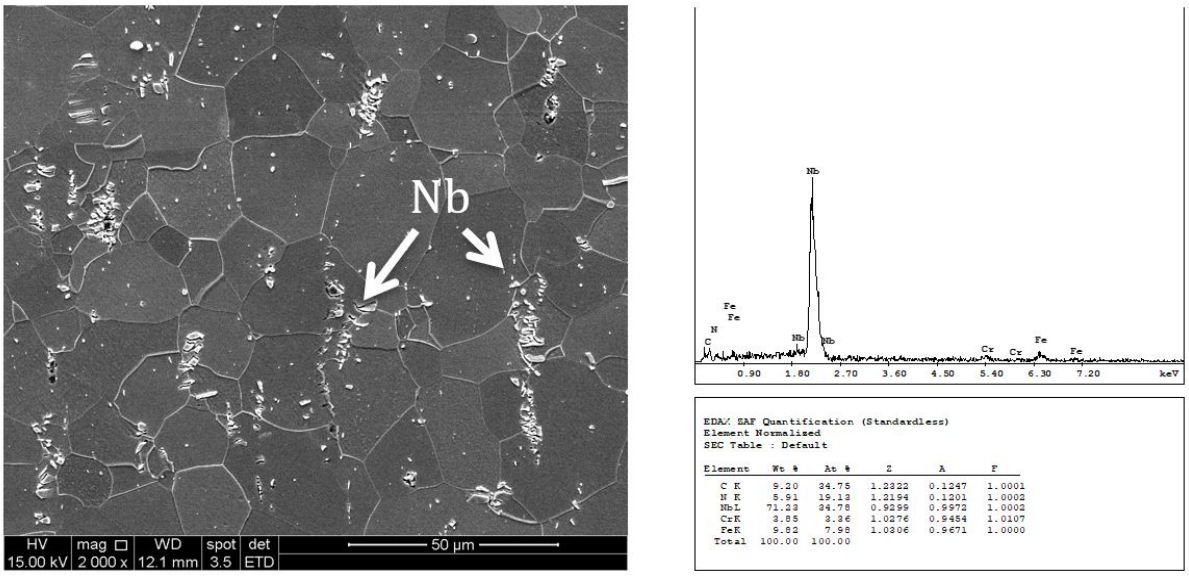

Figure 5. EDS shows Nb precipitates on the base metal of the AISI 430E steel.

Close to the martensite network that lies along the grain boundaries the carbides concentration is reduced by carbon absorption into the martensite. Typically, these carbides concentrate on grain boundaries, but at high temperature C is dissolved in the austenite that transforms to martensite phase during cooling. Thus, the $M_{23}C_6$ precipitates forms mainly inside the grains.

The WM of AISI 430E (Figure 3f) did not show martensite phase due the presence of Nb which suppress the existence of austenite during the welding process, but fine carbides at the grain boundaries and within the grains were present [5].

3.2. Vickers microhardness

Vickers microhardness values for the BM, HAZ and WM are shown in Figure 6. The increase in the amount of martensite and fine precipitates, possible chromium carbides and nitrides, which act as a pinning for dislocation motion, contributes to the increase of hardness of HAZ and WM at AISI 430A. Due to high concentration of martensite and small grains size at the HAZ the microhardness obtained is higher than the microhardness of WM. Individual Vickers microhardness tests were performed at martensite and ferrite matrix and the approximate values found were 330 and 140 HV-0.3, respectively, Figure 7. The value of hardness in the martensite is in agreement with Lippold and Kotecki [15] who reported that the martensite found in ferritic stainless steels are typically of low carbon content with hardeness value around 300 HV.

The WM of AISI 430E showed the highest value of microhardness compared to its BM and HAZ. The dissolution into fine carbides of Nb may have contributed to increase the hardness in this steel region. The microhardness of BM for both steels was very similar.

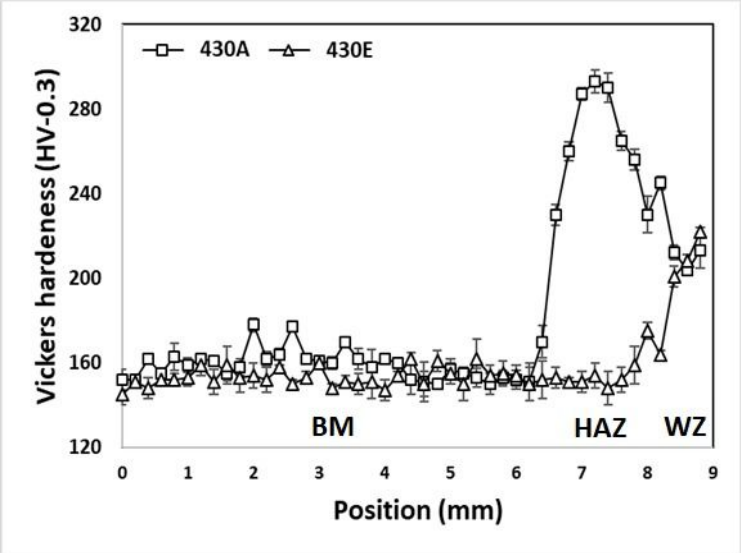

Figure 6. Vickers microhardness values for the BM, HAZ and WZ.

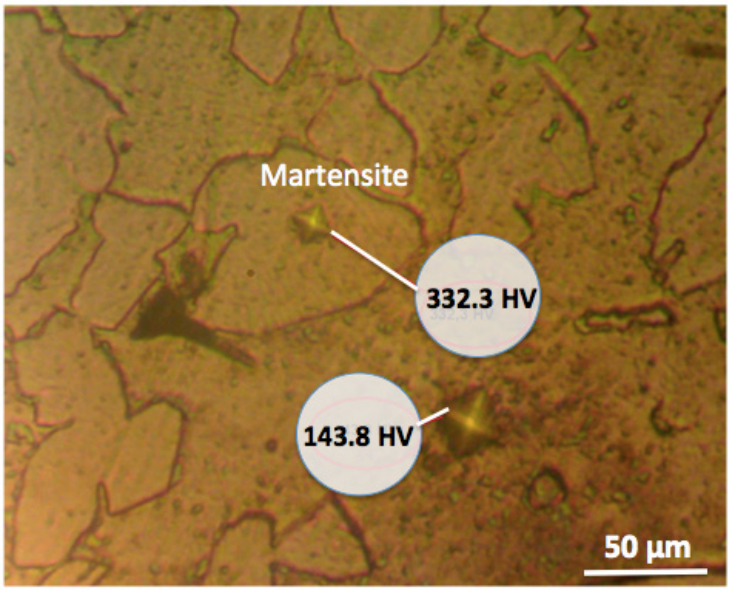

Figure 7. Vickers Microhardness test on HAZ of AISI 430A.

3.3. Intergranular corrosion analysis - DL-EPR

The results of DL-EPR curves are shown in Figure 8, obtained from the BM, HAZ and WZ of AISI 430A and AISI 430E.

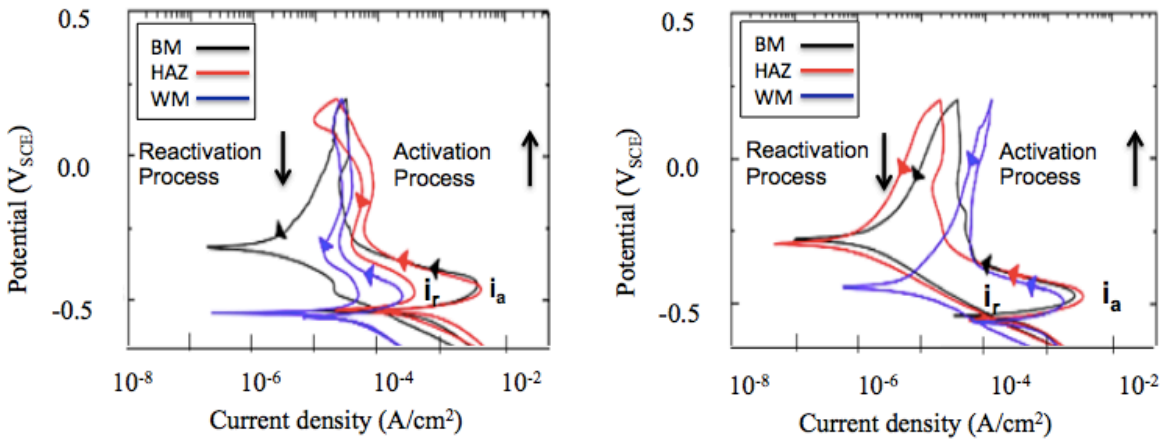

Figure 8. DL-EPR curves for BM, HAZ and WM of AISI 430A(a) and 430E(b).

The BM of AISI 430A, Figure 8a, during the reversion from anode to cathode did not show any sign of a reactivation peak and a continuous decrease in the current density with potential decrease was observed. This indicates that Ir = 0 and could be interpreted as a non-sensitized region with DOS=0. The HAZ and WM of AISI 430A showed recognizable peak of current density of reactivation. According to Pires and Alonos-Falleiros [16], this second peak occurs in samples that have chromium depleted regions, and due to this fact they do not passivate, being susceptible to intergranular corrosion. Therefore, this behavior possibly occurred due to the instability of the passive film. The calculated degree of sensitization of the three regions can be observed in Table 2.

The DOS of HAZ region of the non-stabilized ferritic stainless steel is smaller compared to the WM region, which can be attributed to the high density of martensite, that contribute to a decrease in the DOS. The high DOS of WM region suggests a high precipitation of carbides at the grain boundaries and consequently chromium depletion caused by the weld process. Sidhom et al. [17] observed that values of degree of sensitization above 0.01 indicate sensitized state. In the SEM analysis of WM and HAZ of AISI 430A after the DL-EPR, Figure 9b, c, were found continuous and darkened regions along the ferrite grain, the ditches indicating chromium-carbide depletion in an agreement with the results obtained by the DL-EPR curves.

The SEM of the HAZ and WM of AISI 430E steel presented a dual structure, denoting the presence of grain partially surrounded by ditches, and the BM a step structure which is a result of a difference in crystallographic orientation meaning that the steel is free of carbides precipitation and not susceptible to intergranular corrosion. Thus, the BM, HAZ and WM of AISI 430E Figure 9d-f did not present sensitization what is consistent with the DOS values (DOS = 0). The Nb addition contributes to obtain non-sensitized steel even after welding process.

Table 2. Calculated Degree of Sensitization (DOS) for BM, HAZ and WM. After DL-EPR tests, samples were evaluated by SEM and micrographs are shown in Figure 9a to f.

Steel	Region	Ir/Ia - DOS (%)	Epit (mV_{SCE})	Confidence Interval (95%) Epit (mV_{SCE})
AISI 430A	BM	0	-62 ± 6	± 7
	HAZ	8.8 ±0.3	-38 ± 8	± 9
	WZ	20.3 ± 0.1	-172 ± 11	±13
AISI 430E	BM	0	-64 ± 5	± 6
	HAZ	0	-150 ± 6	± 7
	WZ	0	-97 ± 7	± 8

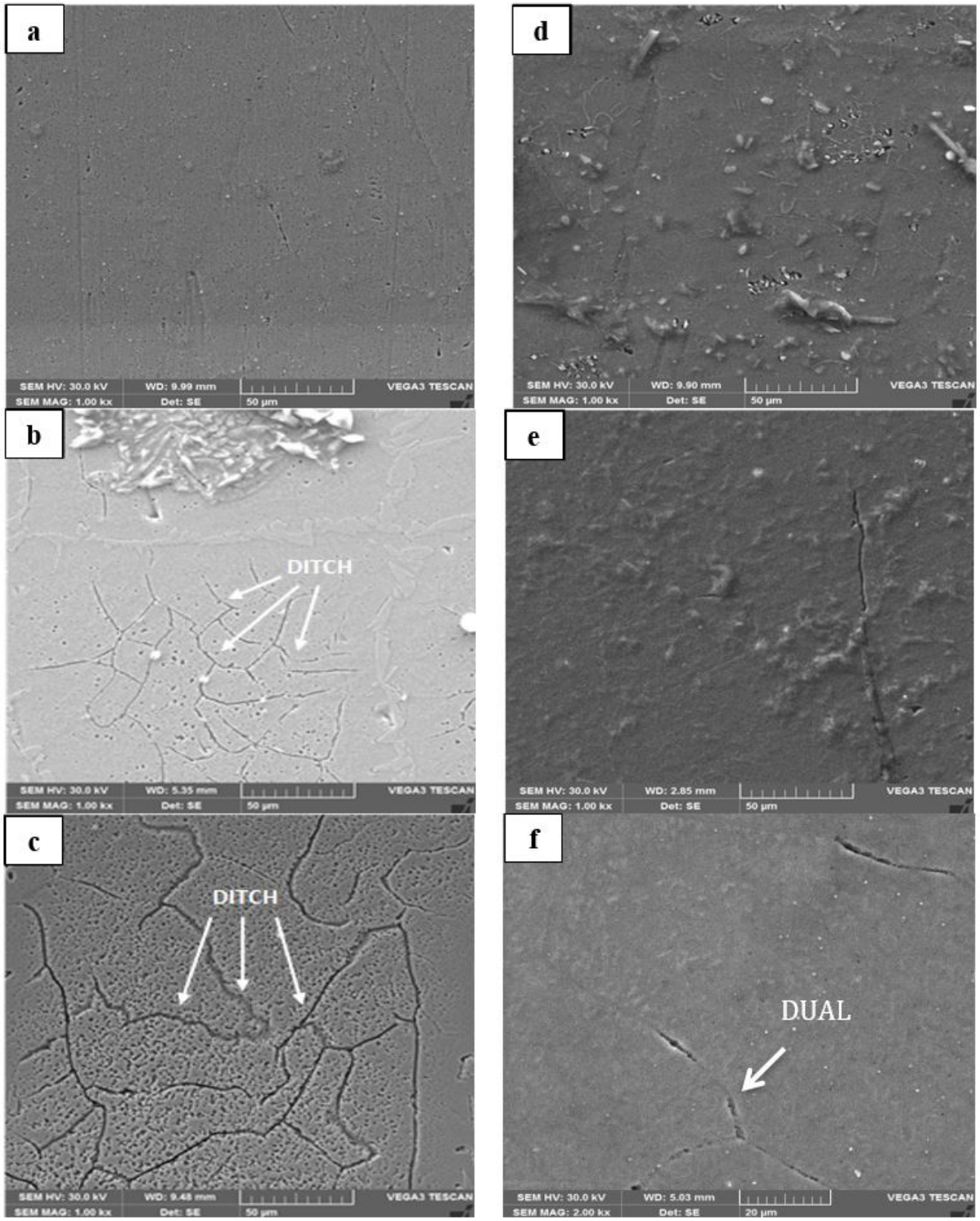

Figure 9. BM (a), HAZ (b) and WM (c) for a ferritic stainless steel 430A – With no addition; BM (d), HAZ (e) and WM (f) for a ferritic stainless steel 430 E - With addition of Nb.

3.4. Pitting corrosion

Pitting potential for all the regions of the AISI 430A and AISI 430E steels resulting from the welding process were obtained by potentiodynamic polarization shown in Figure 10. All the tests were performed in triplicate to ensure reproducibility.

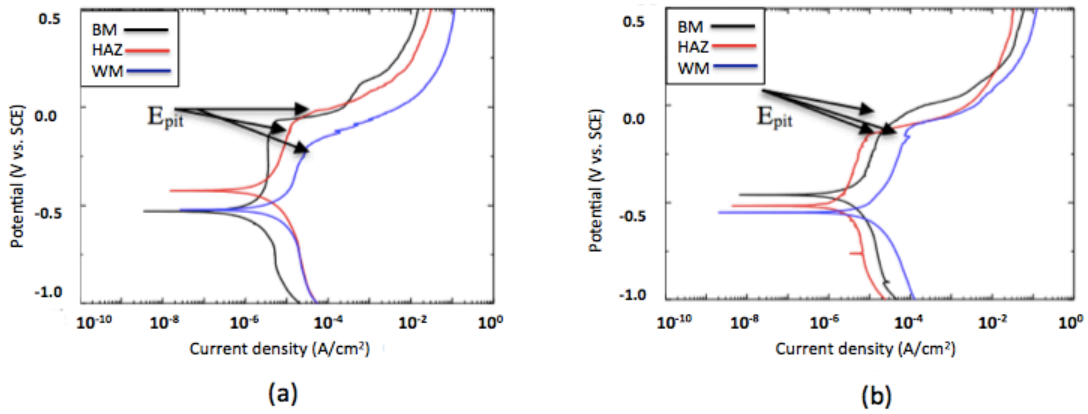

Figure 10. Potentiodynamic polarization curves for 430A (a) and 430E (b).

The pitting potential values for each region are also shown in Table 2. The lowest pitting potential belongs to the WM of the AISI 430A steel (-172 mV_{SCE}), which means that this region exhibited the lowest resistance to pitting corrosion since its occurrence is observed only above Epit. This behavior could be connected to the sensitization effect due to the possible carbide formation ($M_{23}C_6$) at the grain boundaries. This result agrees with Paroni, Alonso-Falleiros and Magnabosco that concluded pitting corrosion potential reduces when the steel has chromium-depleted areas associated with an increase of inter- and intragranular carbides in the ferritic matrix [18]. Thus, sensitization and chromium impoverishment can intensify the pitting corrosion [6].

The pitting potential of HAZ (-38 mV_{SCE}) is higher than the WM and BM regions of the AISI 430A steel presenting the highest resistance to pits formation. This region showed a higher density of martensite network which possible generated a reduction in the formation of $M_{23}C_6$ precipitates. The ferritic stainless steel with Nb (AISI 430E) showed a decrease in pitting potentials in the regions directly affected by the welding process, mainly in the HAZ. Thus the addition of Nb could prevent the sensitization, but was not effective in the pitting corrosion resistance of the steel.

4. Conclusions

Based on the results provided by electrochemical techniques, hardness and SEM in welded AISI 430A and AISI 430E steels; the following conclusions can be drawn:

- The presence of stables Nb carbides contributed to the non-sensitization behavior and no formation of martensite at AISI 430E;
- After welding, the presence of martensite was observed in the HAZ and WM of AISI 430A steel. The increase in the amount of martensite and possible fine precipitates of chromium carbides and nitrides contributes to the increase of hardness of HAZ and WM at AISI 430A. The WM of AISI 430E showed the highest value of microhardness compared to the other regions of the steel due the presence of fine precipitates;
- The base metal with or without Nb showed no degree of sensitization and similar pitting potential. The welding process can modified the pitting potential and the degree of sensitization of HAZ and WM in both steels;
- The addition of Nb could prevent the sensitization, but was not effective in the pitting corrosion resistance of the steel.

Acknowledgements

This work was supported by the Conselho Nacional de Desenvolvimento Científico e Tecnológico – CNPq - Brazil (grant number 478415/2013-3).

References

[1] Amuda MOH, Mridha S. Microstructural features of AISI 430 ferritic stainless steel (FSS) weld produced under varying process parameters. International Journal of Mechanical and Materials Engineering. 2009;4:160-166.

[2] Gordon W, Van Bennekom A. Review of stabilization of ferritic stainless steels. Materials Science and Technology. 1996;12(2):126-131. http://dx.doi.org/10.1179/mst.1996.12.2.126.

[3] Gurram M, Adepu K, Pinninti RR, Gankidi MR. Effect of copper and aluminium addition on mechanical properties and corrosion behaviour of AISI 430 ferritic stainless steel gas tungsten arc welds. Journal of Materials Research and Technology. 2013;2(3):238-249. http://dx.doi.org/10.1016/j.jmrt.2013.02.009.

[4] Alizadeh-Sh M, Marashi SPH, Pouranvari M. Resistance spot welding of AISI 430 ferritic stainless steel: phase transformations and mechanical properties. Materials & Design. 2014;56:258-263. http://dx.doi.org/10.1016/j.matdes.2013.11.022.

[5] Modenesi PJ. Soldabilidade dos aços inoxidáveis. Belo Horizonte: Departamento de Engenharia Metalúrgica e de Materiais, Universidade Federal de Minas Gerais; 2016. p. 17-30.

[6] Bai G, Lu S, Li D, Li Y. Influences of niobium and solution treatment temperature on pitting corrosion behavior of stabilized austenitic stainless steel. Corrosion Science. 2016;108:111-124. http://dx.doi.org/10.1016/j.corsci.2016.03.009.

[7] Sousa CAC, Kuri SE. Relationship between niobium content and pitting corrosion resistance in ferritic stainless steels. Materials Letters. 1995;25(1-2):57-60. http://dx.doi.org/10.1016/0167-577X(95)00134-4.

[8] Sim GM, Ahn JC, Hong SC, Lee KJ, Lee KS. Effect of Nb precipitate coarsening on the high temperature strength in Nb containing ferritic stainless steels. Materials Science and Engineering. 2005;396(1-2):159-165. http://dx.doi.org/10.1016/j.msea.2005.01.030.

[9] Wang L, Song C, Sun F, Li L, Zhai Q. . Microstructure and mechanical properties of 12 wt.% Cr ferritic stainless steel with Ti and Nb dual stabilization. Materials & Design. 2009;30(1):49-56. http://dx.doi.org/10.1016/j.matdes.2008.04.040.

[10] Mallaiah G, Kumar A, Ravinder Reddy P, Madhusudhan Reddy G. Influence of grain refining elements on mechanical properties of AISI 430 ferritic stainless steel weldments: Taguchi approach. Materials & Design. 2012;36:443-450. http://dx.doi.org/10.1016/j.matdes.2011.11.063.

[11] El-El-Kashif E, Asakura K, Koseki T, Shibata K. Effects of boron, niobium and titanium on grain growth in ultra high purity 18% Cr ferritic stainless steel. ISIJ International. 2004;44(9):1568-1575. http://dx.doi.org/10.2355/isijinternational.44.1568.

[12] Kaltenhauser RH. Improving the engineering properties of ferritic stainless steels. Metals Engineering Quarterly. 1971;11(2):41-47.

[13] Aksoy M, Kuzucu V, Korkut MH, Yildirim MM. The effect of niobium and homogenization on the wear resistance and some mechanical properties of ferritic stainless steel containing 17-18 wt.% chromium. Journal of Materials Processing Technology. 1999;91(1-3):172-177. http://dx.doi.org/10.1016/S0924-0136(98)00446-4.

[14] Kang Y, Mao WM, Chen YJ, Jing J, Cheng M. Influence of Nb content on grain size and mechanical properties of 18 wt% Cr ferritic stainless steel. Materials Science and Engineering A. 2016;677:453-464. http://dx.doi.org/10.1016/j.msea.2016.09.080.

[15] Lippold JC, Kotecki DJ. Welding metallurgy and weldability of stainless steels. 1st ed. Vol. 5. Nova Jersey: Wiley- Interscience; 2005. p. 87-140.

[16] Pires RF, Alonos-Falleiros N. Avaliação da corrosão intergranular de aço inoxidável ferrítico através de método de reativação eletroquímica. In: Anais do 59º Congresso Anual Da ABM-Internacional; 2004 Julho 19-22; São Paulo. São Paulo: Tec Art; 2004. p. 482-491.

[17] Sidhom, H., Amadou, T., & Braham, C. (2010). Evaluation by the double loop electrochemical potentiokinetic reactivation test of aged ferritic stainless steel intergranular corrosion susceptibility. *Metallurgical and Materials Transactions A, Physical Metallurgy and Materials Science*, 41(12), 3136-3150. http://dx.doi.org/10.1007/s11661-010-0383-3.

[18] Paroni ASM, Alonso-Falleiros N, Magnabosco R. Sensitization and pitting corrosion resistance of ferritic stainless steel aged at 800 °C. Corrosion. 2006;62(11):1039-1046. http://dx.doi.org/10.5006/1.3278231.